ELSEVIER

Journal of Nuclear Materials 281 (2000) 65–70

journal of nuclear materials

www.elsevier.nl/locate/jnucmat

A method to study deformation mechanisms for irradiated steels using a disk-bend test

E.H. Lee *, T.S. Byun, J.D. Hunn, N. Hashimoto, K. Farrell

Metals and Ceramics Division, Oak Ridge National Laboratory, P.O. Box 2008, Oak Ridge, TN 37831-6376, USA

Received 16 March 2000; accepted 2 May 2000

Abstract

There is considerable interest in understanding how dislocations interact with defect clusters produced by radiation to evaluate and remedy the radiation induced degradation of mechanical properties. In this paper, it is demonstrated that deformation mechanisms for irradiated materials can be studied with small TEM disks by employing a disk-bend method. Results showed that dominant deformation modes in ion-irradiated austenitic steel were planar glide and microtwinning. It was concluded that the disk-bend method will be a powerful tool in studying deformation microstructures of irradiated materials.

1. Introduction

Ductility loss and embrittlement of steels associated with radiation induced defects and helium accumulation have been an important subject of investigation in the fission and fusion reactor materials research communities [1]. Recently, the development of accelerator based spallation neutron sources are underway in the US, Europe, and Japan [2–4]. In such a system, as a result of nuclear reactions, helium will be generated at a rate of ≈200 appm/dpa, which is about 100 times higher than in fission reactor materials and about 10 times higher than in fusion-irradiated materials. Hence, the effects of helium build-up in the target vessel steel have come under intense scrutiny. In recent studies on proton and heavy ion irradiated AISI 316 austenitic stainless steel, a significant finding was that radiation induced hardening was dramatically augmented at high helium concentrations [5,6].

In the past, various in-reactor irradiation experiments have been carried out to study or monitor the radiation effects on structural components subjected to a radiation environment. At the same time, many simulation experiments have been conducted for various Fe–Cr–Ni base austenitic steels using accelerators to understand the radiation induced phenomena [7]. However, most simulation studies were confined to an examination of the radiation induced microstructure of helium implanted 316L austenitic stainless steel [8] and the measurement of surface hardness with a sensitive hardness tester, such as the Nanoindenter® for 316LN austenitic stainless steel irradiated by H, He, and Fe ions in single, dual, and triple ion-beam irradiation modes [9]. Thus far, only a few experiments have been conducted to study the deformation mechanisms for ion irradiated materials (i.e., 304L austenitic stainless steel) [10], mainly because the ion damage is confined to the near-surface region, not to the bulk. Although the deformation microstructure has been examined for various in-reactor irradiated and tensile tested specimens including Fe–Cr–Ni base steels, and Al, Cu, Nb, Mo, Re, and V alloys [11–13], such a process is very time consuming, expensive, and strenuous because of long irradiation time and difficulty in handling radioactive materials. Moreover, a well-designed, systematic study is often difficult in reactor irradiation because of system constraints, such as controlling temperature and dose.

In this work, a method to study deformation mechanisms using a small ion irradiated transmission electron microscopy (TEM) disk is developed for the first time, although many investigators have employed the

* Corresponding author. Tel.: +1-865 574 5058; fax: +1-865 574 0641.

E-mail address: LeeEH@ornl.gov (E.H. Lee).

0022-3115/00/$ - see front matter
PII: S0022-3115(00)00130-6

indentation technique to study mechanical properties in the past [14]. The method involves irradiation of a small steel disk under controlled conditions, deformation of the disk to a desired level by the disk-bend method, electro-chemical thinning of the strained disk to reveal the irradiated and deformed region, and examination of the microstructure. The results show that deformation mechanisms can be studied economically and systematically by employing ion irradiation, with easy variation of irradiation conditions (e.g., temperature, dose, gas atom injection etc.). Thus far, several series of experiments have been conducted to investigate the effects of radiation induced defects on mechanical deformation mechanisms. In this report, a procedure for specimen preparation and test method are described to demonstrate the feasibility of this new approach. An example of the test results is presented to demonstrate the power and convenience of this new approach in studying the effects of radiation on deformation mechanisms.

2. Experimental

One alloy investigated in this experiment was a solution annealed AISI 316LN austenitic stainless steel (Jessop Steel Company Heat # 18474), which is a candidate material for the future spallation neutron source (SNS) target container vessel. The nominal composition of the alloy was, in weight percent, 16.3 Cr, 10.2 Ni, 2.01 Mo, 1.75 Mn, 0.39 Si, 0.009 C, 0.11 N, 0.029 P with the balance Fe. Disks of 3 mm diameter and 0.25 mm thickness were prepared by mechanical and electrochemical polishing prior to irradiation. Irradiation was carried out with 360 keV He^+ ions at 200°C using a 2.5 MV Van de Graaff accelerator at ORNL. The 360 keV ion energy resulted in a maximum gas atom deposition near a depth of 750–850 nm, according to a depth calculation by the computer code, Stopping and Range of Ions in Matter (SRIM, 1998 version) [15]. The 360 keV He^+ ion also produced atomic displacements at a rate of $\simeq 7.5 \times 10^{-5}$ dpa/appm at this depth. The specimen received about 2000 appm or 0.2 at.% helium and 0.15 dpa at the peak damage region. The procedure to calculate dpa is described in Ref. [16].

The irradiated disk was clamped into a recessed circular holder with a central opening area of 1.6 mm diameter, as illustrated in the schematic drawing in Fig. 1. The irradiated side of the disk was placed face-down, and a tungsten carbide (WC) ball of 1 mm diameter was placed on top of the unirradiated side of the TEM disk. A load up to ≈30 N was applied on the WC ball at a strain rate of $\approx 10^{-2}$ per second at room temperature using a Tinius Olsen testing machine until the average plastic strain of the center region of the disk attained about 7%.

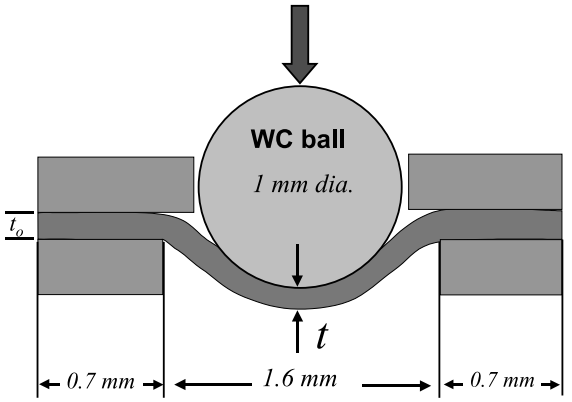

Fig. 1. Schematic drawing of a disk bend setup. The thickness change after deformation was measured by the displacements of the machine cross-head in contact with the WC ball and a LVDT placed underneath the disk.

The average plastic strain (ε_p) was calculated by employing a volume constant criterion and the relation, $\varepsilon_p = \ln(t_0/t)$, where t_0 and t are the thickness of the center region of the disk in contact with the WC ball before and after deformation, respectively. The thickness change after relaxation (zeroing the load) was determined by reading the displacement of the tensile machine cross-head bar in contact with the top of the WC ball and the displacement of a linear variable differential transducer (LVDT) placed underneath the TEM disk.

In this experimental set-up, the irradiated side of the TEM disk surface was strained in multiaxial tension. The irradiated surface strain was more than that at the surface in contact with the WC ball. A comparison of relative displacements of landmarks on the specimen surface before and after disk bend straining indicated that the local strains were not uniform due to varied grain orientations and slip directions. Such uneven strain is also true in a conventional tensile tested specimen, but it is not of great concern because the tensile properties are derived from an average strain of the entire test gauge. However, this inherent variation can be a significant source of uncertainty when a very limited area is examined, as in TEM. In consideration of these uncertainties, the strain at the irradiated surface was estimated to be in the range of 7–13%.

Specimen thinning for TEM was carried out by two methods. First, a thin TEM foil was prepared by electrochemically removing ≃700 nm from the ion bombarded side of the disk and then thinning from the unirradiated side until a perforation occurred. This procedure produced TEM foils with thicknesses of ≃100 nm on average and allowed examination of the microstructure at the peak damage region between 700 and 800 nm of the original depth. Secondly, the

irradiated and deformed TEM disk was Ni-plated electrochemically, sliced across the disk thickness in the ion beam direction, and electrochemically thinned until a perforation occurred across the irradiated region. This cross-sectioned and thinned specimen allowed us to examine the full damage profile and the transition of deformation modes from irradiated to unirradiated areas. Microstructures were examined with a Philips CM12 electron microscope operated at 120 keV and a JEOL FX2000 electron microscope operated at 200 keV. Optical microscopy was also carried out to examine the surface morphology after disk-bend deformation.

3. Results

Microstructures of unimplanted and 0.2 at.% He-implanted TEM disks were examined before and after deformation. Optical microscopy examination revealed a noticeable difference in slip characteristics between the unirradiated and He-implanted specimens as shown in Fig. 2; the bubble-like specks on the surface are stains caused by moisture condensation, which were removed during polishing for TEM foil preparation. The surface morphology of the pristine disk was characterized by numerous very fine slip steps with frequent cross-slip lines, whereas the implanted specimen showed fewer and coarser slip bands. The number of optically visible slip traces, including very faint traces, was about 5 per μm in the pristine specimen. About the same number of slip traces was observed by TEM. One notable observation was that the implanted specimen showed highly localized, large surface steps with very shallow slip traces between them, suggesting that the strain was confined mostly to larger slips and that such localized strain could be a degrading factor on mechanical properties.

Fig. 3 compares the TEM microstructures corresponding to Fig. 2 for the pristine and implanted specimens after deformation. A major deformation feature in the pristine specimen was random glide dislocations and formation of dislocation network cells. Despite the presence of random cross-slip, there was a tendency of dislocations to align along the {1 1 1} slip planes, a characteristic of fcc steels with low stacking fault energy.

At a helium level of 0.2 at.%, bubbles could not be resolved clearly by TEM, although a grainy bubble-like feature at high magnification suggested the presence of small bubbles. However, a high number density of extremely fine black-dots (radiation induced interstitial defect clusters) were present, Figs. 3(b) and 4(d). The deformation mode in the He-implanted specimen was characterized by extensive dislocation pileups on glide planes and formation of microtwins and stacking faults resulting from planar glide (movement of widely separated partial dislocations). TEM diffraction analyses revealed that twin formation occurred exclusively as a result of dislocation glide on {1 1 1} planes. Cross-slip was severely restricted in the presence of radiation induced defects.

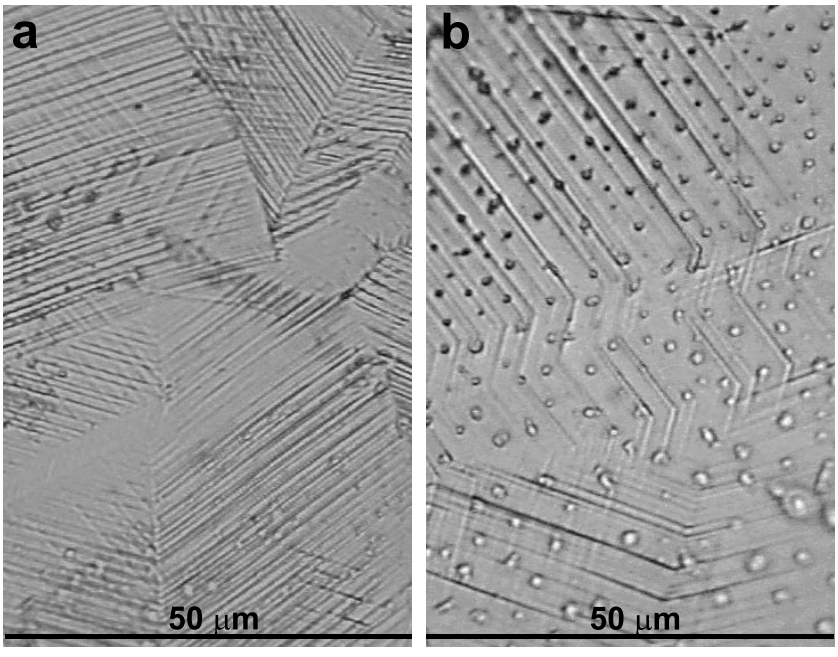

Fig. 2. Optical micrographs of AISI 316 LN austenitic stainless steel after deformation to an average strain of about 7%: (a) unirradiated and (b) implanted with 0.2 at.% helium by 360 keV He-ions at 200°C.

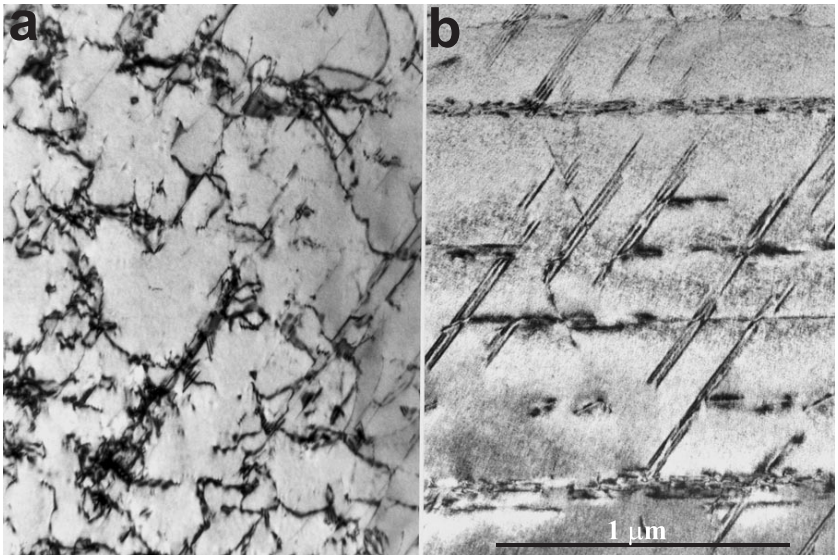

Fig. 3. TEM micrographs of deformation microstructure corresponding to Fig. 2: (a) unirradiated and (b) 0.2 at.% helium implanted with 360 keV He ions at 200°C.

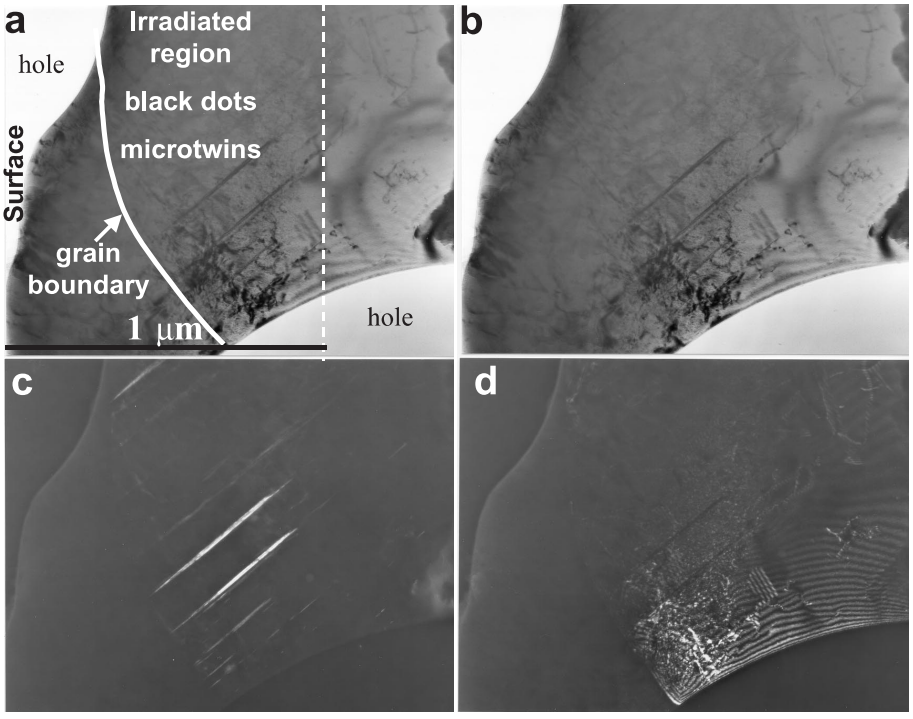

Fig. 4. TEM cross-sectional view of deformation microstructure for the specimen with 0.2 at.% helium implanted with 360 keV He ions at 200°C: (a) description of TEM viewing area; (b) bright field image taken near beam direction $B = [0\,1\,1]$ at $g = 200$ diffracting condition; (c) image taken from twin streaks in diffraction pattern, and (d) weak beam dark field (WBDF) image taken at $g = 200$, $g/5g$ condition.

Fig. 4(a) shows a thin cross-sectioned area with two holes around it because of the uneven polishing among the Ni-plated, He-implanted, and unirradiated bulk regions. The bright field micrograph showed the presence of black-dot defects and deformation microtwins in the He-implanted region (Fig. 4(b)). The dark-field micro-

graph taken from the twin streaks from the diffraction pattern further confirmed the presence of twin bands in the irradiated region (Fig. 4(c)). A weak beam dark field image showed the white strain-contrast spots arising from the black-dots, a few dislocation lines, and a grain boundary in the implanted region (Fig. 4(d)). In the left side of the irradiated grain, twins were also present but not visible because of the difference in grain orientation. A particularly interesting feature was that the deformation twins were confined only to the region where the radiation induced black-dot defects were present, and the twins were not present in the unirradiated region, even in the same grain.

4. Discussions

The deformation mechanism in the pristine specimen was characterized by dislocation multiplication and dislocation network cell formation. Although dislocations tended to align on {1 1 1} glide planes, the presence of randomly distributed dislocations and the slip offsets seen in the optical micrograph indicated that a significant fraction of dislocations cross-slipped during deformation. On the other hand, deformation in the He-implanted specimen was characterized by extensive linear dislocation pileup and microtwin formation. Cross-sectional examination of the irradiated and deformed areas showed that the deformation twins were observed only in the region with radiation induced defects, namely black dot interstitial clusters (perhaps also small helium bubbles), attesting that the twin formation was associated with radiation induced obstacles.

The shear displacement associated with plastic deformation occurred primarily by the motion of dislocations. It is well established that plastic deformation in fcc crystals occurs mainly by dislocation glide on energetically favorable close packed {1 1 1} planes in ⟨1 1 0⟩ directions [17]. Furthermore, in steels with low stacking fault energy such as austenitic stainless steel ($E_{sf} < 10$ J/m^2) [18], ⟨1 1 0⟩ **b** type dislocations tend to dissociate into two ⟨1 1 2⟩ **b** type Schockley partials having a stacking faulted (also twinned) region between them. That is, atoms move by zig-zagging along the energetically favorable valleys (⟨1 1 2⟩ **b**) on close packed {1 1 1} planes instead of directly over the hills (⟨1 1 0⟩ **b**). The partial dislocations repel one another to reduce the stress while the driving force to minimize the stacking faulted surface area between the two partials makes them attract one another. Thus, the spacing between the two leading (zig) and trailing (zag) partials is determined by the forces of repulsion and attraction balance at an equilibrium spacing that depends on the specific stacking-fault energy. The movement of either partial on a different plane would involve energetically unfavorable atomic movements, so the movement of the two widely separated Shockley partial dislocations (planar glide) occurs predominantly on the close packed planes. For these reasons, most slip steps (multiples of the unit dislocation vector **b**) appear straight in stainless steels. In fcc crystals, the close-packed {1 1 1} glide planes are also the coherent twin planes. Therefore, when a layer of atoms is removed from the normal order sequence by dislocation movement, stacking faults and twins are formed as a result of the violation of close packing on the fault plane [17].

Consistent with the mechanisms stated above, most slip traces in the pristine austenitic stainless steel were straight (Fig. 2). However, the presence of slip offsets indicated that cross-slip also occurred. TEM microstructure confirmed that although most dislocation lines aggregated on {1 1 1} planes, various segments of dislocation lines cross-slipped to different planes becoming screw or mixed-type dislocations. As a result, very few stacking faults and twins were observed.

In the He-implanted specimen, however, the alignment of slip traces was enforced, and micro-twins and stacking faults became the dominant deformation microstructures. It is known that cross-slip of an extended screw dislocation around obstacles is difficult, and shear occurs mostly by the successive motion of twinning dislocations, each on a glide plane one interplanar spacing removed from its predecessor [17,18]. Less frequently, however, application of suitably large stress can squeeze the partial dislocations together against a barrier to form a whole dislocation and facilitate cross-slip. Such an incidence often leads to a bifurcation of a channel band and becomes one of the mechanisms of widening a channel band. Clearly, our experimental observations indicated that the restricted dislocation motion on easy glide planes and the limited cross-slip observed in the He-implanted specimen were attributable to radiation induced obstacles (black dots). Although helium bubbles were not visible, probably small bubbles also played a role in restricting dislocation motion. Moreover, stacking faults (twins) themselves are important barriers to dislocation motion, and glide-twinning and twin–twin interaction lead to an opening of a gap in the twin if untwinning occurs successively on twin planes [19].

5. Conclusions

Radiation effects on deformation mechanisms were studied by employing a disk bend method for AISI 316LN stainless steel irradiated with 360 keV He ions at 200°C. The dominant deformation modes in an unirradiated specimen were dislocation multiplication and formation of dislocation network cells, and those in a He-implanted specimen were planar dislocation pileups and the formation of microtwins and stacking faults. Cross-slip occurred readily in unirradiated materials, but the shear deformation was dictated by planar glide

in the He-implanted specimen, suggesting that dislocation motions were confined mostly on glide planes due to the presence of radiation induced obstacles. The combined effects of radiation induced defects and deformation induced microstructure are considered to be a contributing factor to the degradation of mechanical properties of irradiated material.

An important outcome of this experiment is the demonstration that radiation effects on deformation mechanisms can be studied with small TEM disks by employing ion irradiation and a disk-bend test. This method can also be applied to in-reactor irradiated disks for speedy screening tests and for studying the radiation effects on mechanical deformation. At this time, an environment chamber capable of controlling the test temperature from −150°C to 400°C is being installed to study temperature effects. This new approach can be a powerful tool for studying deformation mechanisms of irradiated materials effectively, economically, and systematically under various simulation conditions.

Acknowledgements

This research was sponsored in part by the Division of Materials Sciences and Engineering, Office of Basic Energy Sciences, US Department of Energy, under contract No. DE-AC05-900OR22725, and in part by the NERI Project IWO MSF 99-0072 with UT-Battelle, LLC. The authors thank Drs R.L. Klueh and A.F. Rowcliffe for technical review of the manuscript.

References

[1] Proceedings of the Eight International Conference on Fusion Reactor Materials (ICFRM-8), Sendai, Japan, 26–31 October 1997, J. Nucl. Mater. 258–263, 271&272 (1998).
[2] AccApp'98, American Nuclear Society, La Grange, IL, 1998.
[3] AccApp'99, American Nuclear Society, La Grange, IL, 1999.
[4] Second International Topical Meeting on Nuclear Applications of Accelerator Technology, Gatlinburg, Tennessee, 1998, American Nuclear Society, La Grange Park, Illinois, 20–23 September.
[5] H. Ulmaier, E. Camus, J. Nucl. Mater. 251 (1997) 262.
[6] E.H. Lee, J.D. Hunn, G.R. Rao, R.L. Klueh, L.K. Mansur, J. Nucl. Mater. 271&272 (1999) 385.
[7] E.H. Lee, L.K. Mansur, Metall. Trans. A 23 (1992) 1997.
[8] C.H. Zhang, K.Q. Chen, Y.S. Wang, J.G. Sun, J. Nucl. Mater. 258–263 (1998) 1623.
[9] E.H. Lee, G.R. Rao, J.D. Hunn, P.M. Rice, M.B. Lewis, S.W. Cook, K. Farrell, L.K. Mansur, in: M.S. Wechsler, L.K. Mansur, C.L. Snead, W.F. Sommer (Eds.), Materials for Spallation Neutron Sources, TMS, Warrendale, PA, 1998, p. 57.
[10] S.M. Bruemer, J.I. Cole, R.D. Carter, G.S. Was, Mater. Res. Soc. Symp. Proc. 439 (1997) 437.
[11] M.S. Wechsler, The Inhomogeneity of Plastic Deformation, American Society for Metals, Metals Park, OH, 1971, p. 19 (Chapter 2).
[12] P.D.K. Nathanson, P.J. Jackson, D.R. Spalding, Acta. Metall. 28 (1980) 823.
[13] N. Yamamoto, J. Nagakawa, Y. Murase, H. Shiraishi, J. Nucl. Mater. 258–263 (1998) 1628.
[14] P. Jung, H. Ullmaier (Eds.), Miniaturized specimen for testing of irradiated materials, in: Proceedings of the IEA International Symposium, Forschungszentrum Jülich GmbH, Germany, 1995.
[15] J.F. Ziegler, J.P. Biersack, U. Littmark, The Stopping and Range of Ions in Solids, Pergamon, Oxford, 1985.
[16] E.H. Lee, Nucl. Instrum. and Meth. B 151 (1999) 29.
[17] J.P. Hirth, J. Lothe, Theory of Dislocations, McGraw-Hill, New York, 1968 (Chapters 10 & 23).
[18] R.W. Hertzberg, Deformation and Fracture Mechanics of Engineering Materials, Wiley, New York, 1976 (Chapter 3).
[19] P. Müller, C. Solenthaler, Mater. Sci. Eng. A 230 (1997) 107.